# Acidity of a Cu-Bound Histidine in the Binuclear Center of Cytochrome *c* Oxidase

**Elisa Fadda, Nilmadhab Chakrabarti, and Régis Pomès***

*Structural Biology and Biochemistry, The Hospital for Sick Children, and Department of Biochemistry, University of Toronto, Toronto, Ontario, Canada*

Cytochrome *c* oxidase (CcO) is a crucial enzyme in the respiratory chain. Its function is to couple the reduction of molecular oxygen, which takes place in the $Fe_{a3}$−$Cu_B$ binuclear center, to proton translocation across the mitochondrial membrane. Although several high-resolution structures of the enzyme are known, the molecular basis of proton pumping activation and its mechanism remain to be elucidated. We examine a recently proposed scheme (*J. Am. Chem. Soc.* **2004,** *126,* 1858; *FEBS Lett.* **2004,** *566,* 126) that involves the deprotonation of the $Cu_B$-bound imidazole ring of a histidine (H291 in mammalian CcO) as a key element in the proton pumping mechanism. The central feature of that proposed mechanism is that the $pK_a$ values of the imidazole vary significantly depending on the redox state of the metals in the binuclear center. We use density functional theory in combination with continuum electrostatics to calculate the $pK_a$ values, successively in bulk water and within the protein, of the Cu-bound imidazole in various Cu− and Cu−Fe complexes. From $pK_a$s in bulk water, we derived a value of −266.34 kcal·$mol^{-1}$ for the proton solvation free energy ($\Delta G_{sol}^{H^+}$). This estimate is in close agreement with the experimental value of −264.61 kcal·$mol^{-1}$ (*J. Am. Chem. Soc.* **2001,** *123,* 7314), which reinforces the conclusion that $\Delta G_{sol}^{H^+}$ is more negative than previous values used for $pK_a$ calculations. Our approach, on the basis of the study of increasingly more detailed models of the CcO binuclear center at different stages of the catalysis, allows us to examine successively the effect of each of the two metals' redox states and of solvation on the acidity of imidazole, whose $pK_a$ is approximately 14 in bulk water. This analysis leads to the following conclusions: first, the effect of Cu ligation on the imidazole acidity is negligible regardless of the redox state of the metal. Second, results obtained for Cu−Fe complexes in bulk water indicate that Cu-bound imidazole $pK_a$ values lie within the range of 14.8−16.6 throughout binuclear redox states corresponding to the catalytic cycle, demonstrating that the effect of the Fe oxidation states is also negligible. Finally, the low-dielectric CcO proteic environment shifts the acid−base equilibrium toward a neutral imidazole, further increasing the corresponding $pK_a$ values. These results are inconsistent with the proposed role of the Cu-bound histidine as a key element in the pumping mechanism. Limitations of continuum solvation models in $pK_a$ calculations are discussed.

## 1. Introduction

Cytochrome *c* oxidase (CcO) is the terminal enzymatic complex in the mitochondrial respiratory chain. Its catalytic function is to reduce $O_2$ to $H_2O$ and to harness the free energy released by that reaction to pump protons across the mitochondrial inner membrane. The electrochemical gradient generated across the membrane by the excess protons is ultimately used to drive ATP synthesis.[1-5] The high efficiency of CcO rests precisely on the balanced coupling between proton pumping and the redox reaction:

$$O_2 + 4e^- + 8H^+ \rightarrow 2H_2O + 4H^+ \qquad (1)$$

The oxygen reduction takes place in the binuclear center, which consists of a high-spin Fe $heme_{a3}$ and a $Cu_B$, in the enzyme active site (see Figure 1). Two distinct proton uptake pathways connect the binuclear center to the matrix side of the mitochondrial membrane,[5-8] namely the D-channel and the K-channel, which owe their names to conserved aspartate and lysine residues, respectively. It is generally accepted that seven of the eight protons involved in the catalytic cycle follow the D-channel from the matrix to the active site, while only one proton adopts the K-channel.[9,10] Four of the eight protons are consumed in the redox reaction to produce two water molecules (chemical protons), while the other four are translocated through the enzyme (pumped protons). All protons are transported to the CcO active site, from which they are directed either toward the binuclear center or toward the exit pathway. A detailed picture of the mechanism underlying this selective proton distribution is a matter of debate.[11-15] The analysis of the many available crystallographic structures of CcO does not show any specific pathway connecting the mouth of the D-channel to the binuclear center or leading protons to the exterior side of the membrane. It is thought that both chemical and pumped protons are relayed within the active site cavity through dynamic networks of hydrogen-bonded water molecules.[7,13,16-18] Furthermore, the direction of proton transfer through hydrogen-bond networks has been suggested to be coupled to the electron transfer to the $heme_{a3}$−$Cu_B$ binuclear center.[13] Recent studies have proposed the direct involvement of one of the $Cu_B$ histidine ligands (i.e., H291 in bovine heart CcO, or H334 in *Rhodobacter sphaeroides* CcO) as a proton loading site in the pumping mechanism.[7,11,14,15,19] In these mechanisms, the protonation state of $N_{\delta 1}$ in H291 is assumed to depend on the redox state of the

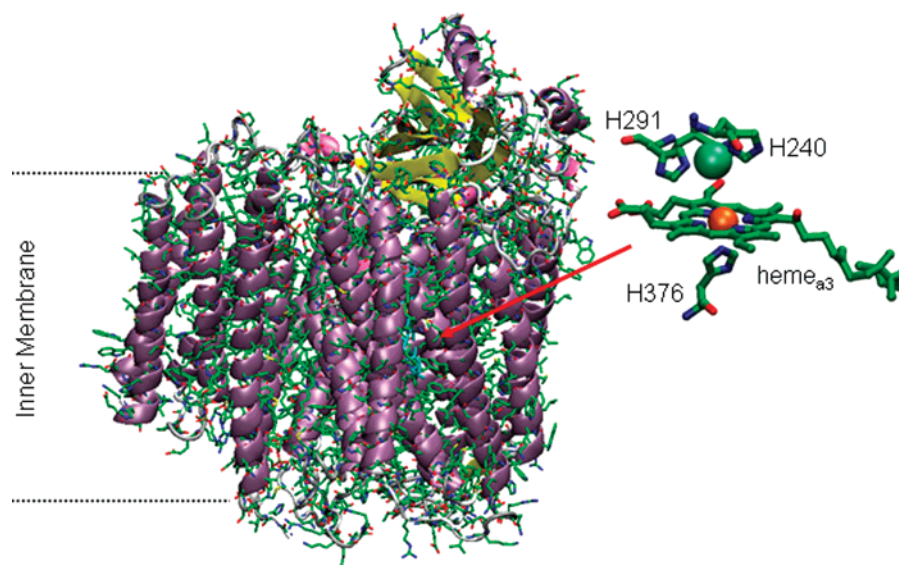* Corresponding author. E-mail: pomes@sickkids.ca.

**Figure 1.** Subunit A of cytochrome *c* oxidase (CcO) from *Rhodobacter sphaeroides* (PDB structure 1M56, ref 6). The residues in the binuclear center are shown in detail at the top-right corner. The numbering of all residues correspond to mammalian CcO; Cu is shown in teal and Fe in orange. The location of the active site within CcO is indicated by an arrow.

metals in the binuclear center. Wikström proposed that the protonation and deprotonation of the histidine side chain is coupled to the dissociation of its imidazole ring from $Cu_B$.[11] An alternative scheme[7,14,15,19] entails that H291 remains ligated to $Cu_B$ and that deprotonation at the $N_{\delta 1}$ position causes the formation of an imidazolate anion (i.e., $Cu_B-ImH \rightarrow Cu_B-Im^-$). This hypothesis was proposed on the basis of continuum electrostatic calculations of CcO.[14,15] A key feature of that proposal is that the entry of a chemical proton in the active site, which converts an $OH^-$ ligand of $Cu_B$ to $H_2O$, causes the $pK_a$ of H291 to drop, leading to the deprotonation of $N_{\delta 1}$.

Although the deprotonation of imidazole, which produces an imidazolate anion, is not possible in bulk water ($pK_a \approx 14$),[20-22] the presence of a metal-coordinated imidazolate anion has recently been determined experimentally in the iron−sulfur protein of the cytochrome $bc_1$ complex.[23] In this system, the imidazolate ring of one of the two Fe-coordinated histidines is hydrogen bonded to the ubiquinol substrate and presumably represents the redox-linked protonation site. A transient endiol−imidazolate complex was also identified as a probable intermediate in the catalytic mechanism of triosephosphate isomerase.[24] The likelihood of the formation of a Cu-bound imidazolate in the CcO active site can be addressed computationally by using a suitable quantum mechanical (QM) approach on an appropriate model system. In this study, we use density functional theory (DFT) in combination with continuum electrostatics to examine the dependence of the Cu-bound imidazole $pK_a$ on the redox state of different Cu and Cu−Fe complexes. Our approach is based on the analysis of the Cu-bound imidazole acidity in increasingly larger systems modeled after the CcO binuclear center at various stages of the catalytic cycle. A schematic depiction of the main steps of the reduction of $O_2$ in the binuclear center, and the proposed connection to the H291 deprotonations,[14] are shown in Figure 2. The fully reduced state of the binuclear center, defined as the "R" state, will be considered here as the starting point of the catalytic cycle. An $O_2$ enters the active site and binds to the metals, forming a "peroxy" (P) state (not shown). The tyrosine (Y244) cross-linked to His240 forms a radical by releasing a hydrogen atom, which helps cleaving the peroxy bond.[25-27] The first electron transfer from the $heme_a$ allows the formation of a negatively charged tyrosine (indicated in Figure 2 as $YO^-$ in the $P_r$ state). In the

"ferryl" state (F) the first chemical proton ($H_{In}^+$) accesses the binuclear center and saturates Y244. The latter remains neutral throughout the following steps of the catalytic cycle.[28] In the transition between the F and $F_p$ states, a chemical proton enters the binuclear center and converts the hydroxyl $Cu_B$ ligand into water, increasing the total charge of the site from +1 to +2. That stage of the catalytic cycle is supposedly connected to the first deprotonation of the His291 imidazole ring. The next proton entering the active site reloads the His291 $N_{\delta 1}$ position. A dismutation leads to the formation of the H′ state. The transition between the H′ and O states is connected to a second deprotonation of H291. In the E state, the first water molecule produced in the redox reaction leaves the binuclear center and the redox state of $Fe_{a3}$ changes from III to II. Here, the fourth and last chemical proton enters the active site and saturates the hydroxyl ($E_p$ state), triggering the third His291 deprotonation. The next incoming proton reloads the $N_{\delta 1}$ position, closing the catalytic cycle. In the original article proposing the deprotonation of His291, the catalytic step connected to the fourth pumping event was not clearly identified.[14]

The complexes studied, shown schematically in Figure 3, were designed to represent stages of the CcO catalytic cycle presumably connected to the Cu-bound imidazole deprotonations. First, we determined the $pK_a$ values in bulk water for simple $[ImH]_3Cu^M-L$ models (where L indicates the fourth ligand, i.e $H_2O$ or $OH^-$, and M indicates the oxidation state of Cu, i.e., I or II). The results on these complexes show the effect of the redox states of the central Cu on the acidity of an isolated imidazole. The effect of the Fe porphyrin was added successively by studying more complex systems where various Fe oxidation states (i.e. II, III, IV) and various intermetal ligands were considered. Last, we calculated the $pK_a$ of the imidazole ring as a $Cu_B$ ligand in the binuclear center of CcO to assess the effect of the low dielectric proteic environment.

The calculation of absolute $pK_a$ values of species in solution is a delicate task, which necessitates the use of high-level QM methods capable of attaining chemical accuracy (average absolute error of about 0.1 eV (or 2 kcal·mol$^{-1}$) against the G2 thermochemical data set.[29]). The treatment of solvation represents the least reliable aspect of $pK_a$ calculations. The expected limits of accuracy range within 2−5 kcal·mol$^{-1}$.[30] To gauge

Acidity of a Cu-Bound Histidine in Cytochrome *c* Oxidase

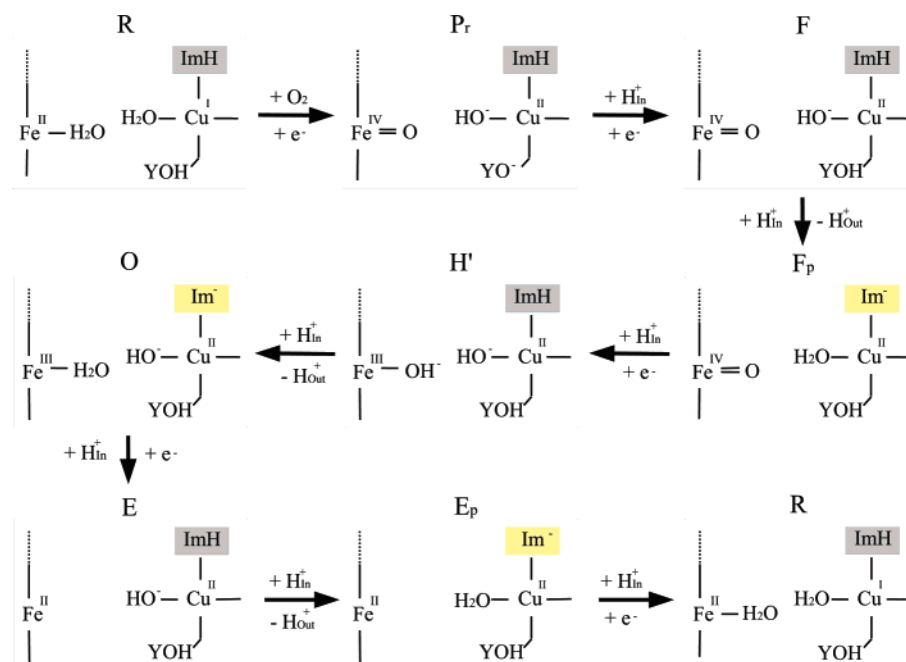*J. Phys. Chem. B, Vol. 109, No. 47, 2005* **22631**



**Figure 2.** Proposed main steps of the reduction of $O_2$ to $H_2O$ in the binuclear center of CcO. The heme$_{a3}$ is represented by the central Fe atom and by a line defining the porphyrin ring. Only the Cu$_B$ histidine ligand side chain undergoing deprotonation is shown. The protonated and deprotonated forms of imidazole are indicated as ImH and Im$^-$, respectively. Catalytic states are defined by a letter shown on top of each frame, according to the commonly used nomenclature.[11,15] The protons entering and exiting the binuclear center are indicated as $H_{In}^+$ and $H_{Out}^+$, respectively.
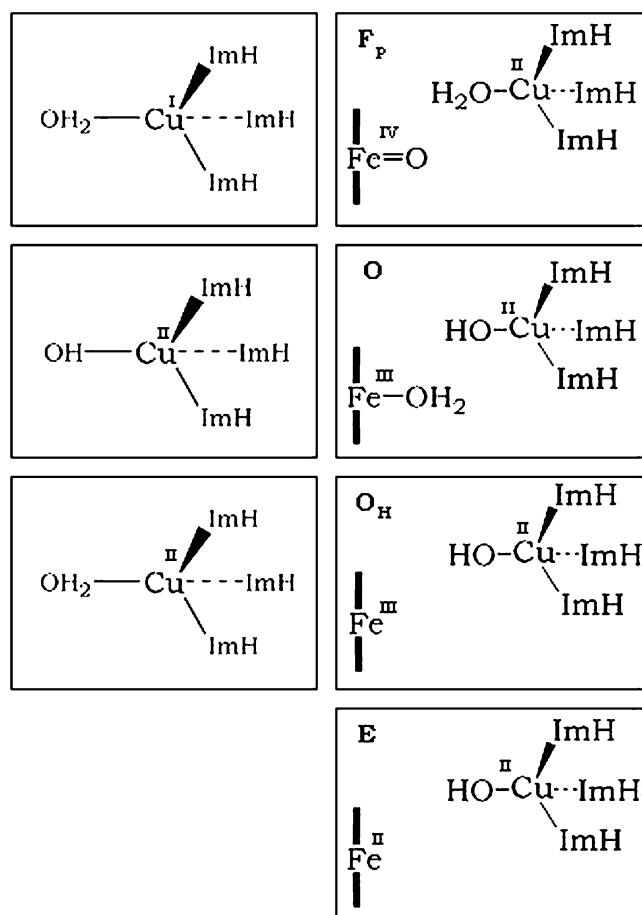


**Figure 3.** Left Cu− and right Cu−Fe complexes studied. The catalytic states of CcO corresponding to the Cu−Fe models are indicated at the top-left corner.

the dependence of p$K_a$ values on the level of theory used to describe solvation, an SCF generalized Born (GB) model and a post-SCF Poisson−Boltzmann (PB) approach are used to determine the solvation free energy in bulk water. Furthermore, tests on acid−base couples for which the solvation free energy is known experimentally show the limitations of GB and PB methods in the treatment of ionic species.

The Cu-bound histidine p$K_a$ values are calculated within CcO by using PB continuum electrostatic calculations. In this highly inhomogeneous environment, the p$K_a$s must be determined through a thermodynamic scheme that includes explicitly the contribution of proton solvation free energy ($\Delta G_{sol}^{H^+}$). Many experimental and computational studies[31−35] have focused on the determination of $\Delta G_{sol}^{H^+}$, and the values reported therein cover a range of 12.0 kcal·mol$^{-1}$ (from −252.6 to −264.6 kcal·mol$^{-1}$). Because of this large range of uncertainty, and for consistency in our results, we estimated $\Delta G_{sol}^{H^+}$ based on the p$K_a$ values that we calculated in bulk water (see Section 2 for details). We obtained $\Delta G_{sol}^{H^+} = -266.340$ kcal·mol$^{-1}$, close to the value of −264.61 kcal·mol$^{-1}$ published by Liptak and Shields,[31] which corresponds to the lowest value in the range of the proton solvation free energies reported in the literature. Our estimate reinforces the conclusion that $\Delta G_{sol}^{H^+}$ is more negative than previous values used for p$K_a$ calculations.

Our calculations show that the acidity of the Cu$_B$-bound imidazole ring in the complexes studied does not depend significantly on the redox state of the metals. The p$K_a$s of the Cu-bound imidazole ring in bulk water vary between 14.8 and 16.6 for the large Cu−Fe complexes around the catalytic cycle. The low dielectric environment of the protein shifts the equilibrium toward the protonated (neutral) form of the Cu-bound histidine, increasing the p$K_a$ values. The implications of these results on the proposed CcO pumping mechanism are analyzed. In two recent publications,[36,37] the p$K_a$ values of imidazole ligands in Cu complexes and in Cu$_B$−heme$_{a3}$ models were evaluated by using an approach similar to ours. However, fundamental differences in the p$K_a$ calculation methodology, which will be discussed in detail in the following sections, lead us to radically different conclusions.
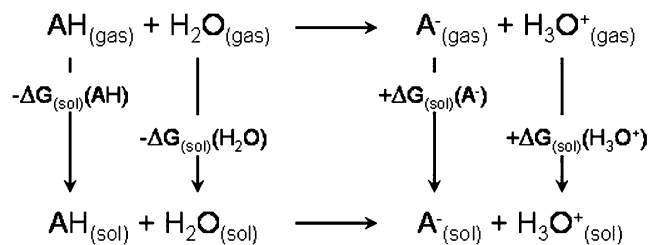
**Figure 4.** Thermodynamic cycle used to determine the p$K_a$ of the species AH. $\Delta G_{sol}$ represents the free energy of solvation.

## 2. Computational Method

**2.1. p$K_a$ Calculations from First Principles.** The thermodynamic cycle commonly used to calculate the acidity of a chemical group AH is shown in Figure 4. On the basis of that cycle, the p$K_a$ can be expressed through the equation:

$$pK_a^{AH} = \frac{(\Delta G_{gas}^{AH} + \Delta\Delta G_{sol}^{AH})}{2.303RT} \quad (2)$$

where $T = 298$ K and $R$ is the molar gas constant. The gas-phase deprotonation free energy ($\Delta G_{gas}^{AH}$) is given by

$$\Delta G_{gas}^{AH} = \Delta H_{gas}^{AH} + \Delta G_{Th}^{AH} + H_{trans}^{H^+} + \Delta(pV) - T[S^{H^+}] \quad (3)$$

It comprises the gas-phase deprotonation energy ($\Delta H_{gas}^{AH}$), a vibrational term ($\Delta G_{Th}^{A,H}$), the proton translational energy ($H_{trans}^{H^+} = {}^3/_2 k_B T$), a term accounting for the change of volume during the reaction ($\Delta(pV) = k_B T$), and the entropic contribution ($S^{H^+}$) to the proton gas-phase energy (7.8 kcal·mol$^{-1}$ according to the Sackur–Tatrode equation[38]). $\Delta H_{gas}^{AH}$ and $\Delta G_{Th}^{AH}$ can be evaluated to high accuracy by first principle calculations. The solvation free energy ($\Delta\Delta G_{sol}^{AH}$ in eq 2) is given by

$$\Delta\Delta G_{sol}^{AH} = \Delta G_{sol}^{A^-} + \Delta G_{sol}^{H^+} - \Delta G_{sol}^{AH} \quad (4)$$

Both $\Delta G_{sol}^{A^-}$ and $\Delta G_{sol}^{AH}$ are usually evaluated through self-consistent continuum solvation methods.[31,39] The proton solvation free energy ($\Delta G_{sol}^{H^+}$) represents an elusive quantity, which is very difficult to determine experimentally and to calculate reliably.[40,41] Indeed, the available experimental[31–34] and calculated[35] values reported for $\Delta G_{sol}^{H^+}$ vary between $-252.6$ and $-264.6$ kcal·mol$^{-1}$. A deviation of only 1.4 kcal·mol$^{-1}$ in any of the free energy contributions appearing in the numerator of eq 2 causes the p$K_a$ to shift by 1 unit. Hence, by taking into account $\Delta G_{sol}^{H^+}$ in the thermodynamic cycle, one can only determine acidities with an uncertainty of approximately 9 p$K_a$ units. Ultimately, the p$K_a$s determined through this method are linearly dependent on the choice of the "best" value for $\Delta G_{sol}^{H^+}$.

The use of an alternative scheme that circumvents the problem of accounting for proton solvation has proven to be quite successful, leading to an accuracy within half of a p$K_a$ unit for carboxylic acids.[42] Within this framework, shown in Figure 5, the unknown p$K_a$ of an acid AH is determined relative to that of the known p$K_a$ of another species, BH

$$pK_a^{AH} = pK_a^{BH} + \frac{(\Delta\Delta G_{gas}^{ref} + \Delta\Delta G_{sol}^{ref})}{2.303RT} \quad (5)$$

where

$$\Delta\Delta G_{gas}^{ref} = (\Delta H_{gas}^{AH} + \Delta G_{Th}^{AH}) - (\Delta H_{gas}^{BH} + \Delta G_{Th}^{BH}) \quad (6)$$
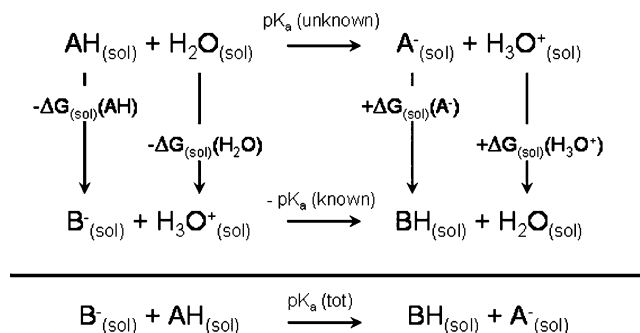


**Figure 5.** Relative scheme for the calculation of the p$K_a$ of species AH. p$K_{a1}$ is the unknown value to determine, p$K_{a2}$ is the known experimental value of the species BH.

and

$$\Delta\Delta G_{sol}^{ref} = (\Delta G_{sol}^{A^-} - \Delta G_{sol}^{AH}) - (\Delta G_{sol}^{B^-} - \Delta G_{sol}^{BH}) \quad (7)$$

The proton solvation free energy is implicitly taken into account by the introduction of p$K_a^{BH}$ as a known constant in eq 5. The p$K_a$ values calculated according to this scheme are independent of the chosen reference (BH). Therefore, in principle, any type of acid BH can be selected. However, limitations in the accuracy of continuum solvation models in describing ionic species accurately can be the cause of additional errors.

**2.2. Model Systems.** The p$K_a$ values of an imidazole ligated to Cu were determined in several complexes modeled after the binuclear center of CcO in catalytic stages proposed[14] to be connected to H291 deprotonation (see Figure 3). We first calculated the p$K_a$ of imidazole (ImH) as a ligand in [ImH]$_3$Cu$^M$L-type complexes, where the superscript $M$ indicates the oxidation state of the metal, while L indicates the fourth ligand (H$_2$O or OH$^-$). From now on, we will refer to this type of complex as the "Cu model". From the CcO catalytic cycle shown in Figure 2, we selected three Cu models for the p$K_a$ calculation, namely: [ImH]$_3$Cu$^I$H$_2$O, [ImH]$_3$Cu$^{II}$H$_2$O (shown as structure a in Figure 6), and [ImH]$_3$Cu$^{II}$OH.

The effect of the Fe porphyrin on the p$K_a$ at a close distance to the Cu center (4.82 Å in *Rhodobacter sphaeroides* CcO, PDB code 1M56, ref 6) is then studied in larger model complexes, which we will refer to as the "Cu−Fe models". [ImH]$_3$ Cu$^{II}$−H$_2$O···O═Fe$^{IV}$[(porph)NH$_3$] is modeled after the F-state of the binuclear center. Two systems are modeled on the O-state, [ImH]$_3$ Cu$^{II}$−OH···H$_2$O−Fe$^{III}$[(porph)NH$_3$] (shown as structure b in Figure 6), and [ImH]$_3$ Cu$^{II}$−OH···Fe$^{III}$[(porph)NH$_3$], respectively, with and without the water molecule ligated to Fe. For the latter model, both antiferromagnetic (S = 2), and ferromagnetic (S = 3) coupling between the two metals are considered to assess the influence of spin coupling on ImH acidity. Last, [ImH]$_3$ Cu$^{II}$−OH···Fe$^{II}$[(porph)NH$_3$] represents the E state. In all complexes, the apical ligand NH$_3$ of the heme group replaces a His side chain. For both Cu−Fe and Cu models, the acidic proton belongs to N$_{\delta 1}$ (indicated by an asterisk in Figure 6). The imidazole that is deprotonated corresponds to H291 in the CcO binuclear center.

Calculations in bulk water were carried out by using the relative scheme depicted in Figure 5. The evaluation of the solvation free energy ($\Delta\Delta G_{sol}^{ref}$ in eq 5) represents the least reliable step in this calculation, especially for the characterization of ionic species. To assess the dependence of the p$K_a$ values on the solvation model used, we determined $\Delta\Delta G_{sol}^{ref}$ for acid−base couples for which $\Delta\Delta G_{sol}^{ref}$ is known experimentally. The results obtained with two continuum models, a self-consistent

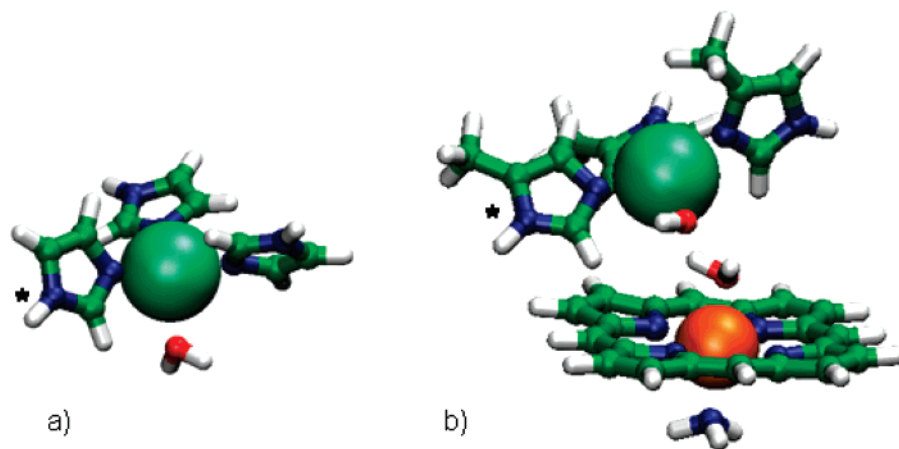**Figure 6.** (a) $[ImH]_3Cu^{II}-H_2O$ complex, and (b) $[ImH]_3Cu^{II}-OH\cdots H_2O-Fe^{III}[(porph)NH_3]$ complex. Cu and Fe atoms are shown in teal and in orange, respectively. The imidazole which undergoes deprotonation is indicated by an asterisk.

generalized Born (GB) model and a Poisson−Boltzmann (PB) post-SCF approach, were compared to the experimental data. This analysis allows us to gauge the level of accuracy attainable for the p$K_a$ value in neutral and ionic species. Furthermore, it allows us to choose as reference equilibrium for the relative scheme (i.e., BH → B$^-$ + H$^+$, see Figure 5) the acid−base couple whose solvation energy is described most accurately by both solvation models.

For the calculations in CcO, one cannot use the relative scheme shown in Figure 5, simply because the p$K_a$ of any acid that could serve as reference BH is not known in the CcO proteic environment. Therefore, we have to rely instead on the thermodymamic cycle depicted in Figure 4. Accordingly, the p$K_a$s are determined through eq 2 and 3. Although the calculations of the imidazole acidity in the protein interior are designed to reproduce most closely the effect of such a complex environment, it is necessary to keep in mind that these p$K_a$ values are linearly dependent on the choice of the "best" value for the proton solvation free energy. In view of this problem and for consistency of the results, we chose to determine $\Delta G_{sol}^{H^+}$ via eq 4 based on the p$K_a$s obtained for Cu and Cu−Fe models in bulk water. More specifically, $\Delta G_{sol}^{H^+}$ was obtained by plugging into eq 4 calculated values for $\Delta G_{sol}^{A^-}$ and $\Delta G_{sol}^{AH}$, together with the value of $\Delta\Delta G_{sol}^{AH}$ obtained from the thermodynamic cycle depicted in Figure 5. The value we obtained ($-266.340$ kcal·mol$^{-1}$) was then used to evaluate the Cu-bound imidazole ring acidity in the protein.

**2.3. Calculation Details.** The initial coordinates for all the models studied were taken from the X-ray structure of CcO from *Rhodobacter sphaeroides*, PDB code 1M56.[6] The different ligands (i.e., H$_2$O, OH$^-$, and O) present at different stages of the catalytic cycle were added manually to the initial structures. The coordinates of all Cu−Fe and Cu models are given as Supporting Information. All open-shell calculations were performed with unrestricted hybrid DFT, namely with the B3LYP exchange-correlation (xc) functional (U-B3LYP).[44] Because of the small influence of spin contamination that may be introduced by the exact HF exchange in B3LYP, it is important to underline that, for all SCF-converged calculations, the expectation value of the total spin $\langle S^2 \rangle$ differs from S(S + 1) by less than 10%.

All protonated and deprotonated Cu models were fully optimized at the 6-31G(1p,1d) level. The electrostatic gas-phase contributions and the vibrational analysis were performed with an *all*-electron TZV(1p,1d) basis set. For the Cu−Fe complexes, all degrees of freedom of the protonated species were relaxed to a gradient convergence threshold of 0.01. This initial step

allowed the internal structure to adapt to the addition of the ligands and to the redox state of the metals. This procedure did not lead to significant deviations from the original X-ray structure of the binuclear center. For these large complexes, the deprotonation is assumed to be instantaneous; therefore, the structure of the deprotonated form is assumed to be identical to that of the protonated form. This assumption is supported by the good agreement observed between the p$K_a$ values obtained for the large Cu−Fe complexes and the Cu models, which were optimized in both protonated and deprotonated forms (see Section 3).

Geometry optimizations on the Cu−Fe models were performed with SBKJC effective core potentials (ECP) for all heavy atoms,[45,46] while valence electrons were described at the 4-31G level. The electrostatic gas-phase terms were determined with a LACV3P(1p,1d) basis set,[47] which entails ECPs for Cu and Fe, and a TZV(1p,1d) quality basis set for all electrons in H, C, N, and O atoms, and valence electrons in the metals. The $\Delta G_{Th}$ terms were assumed to be equal to the ones calculated for the Cu models. Because deprotonation can be considered as a relatively localized phenomenon, and because the Cu model represents a wide enough portion of the Cu−Fe model, this approximation is reasonable. Solvation free energies for Cu models were determined by using two different levels of theory: a self-consistent generalized Born (GB) approximation based on CM3 model charges,[48,49] calculated at the B3LYP// 6-31G(1d) level, and a continuum electrostatic method based on the Poisson−Boltzmann (PB) equation.[50] The latter requires the calculation of the point charges fitted to the electrostatic potential (ESP). Here, these point charges are determined with the Singh−Kollman method,[51] also at the B3LYP//6-31G(1d) level. This protocol was chosen for the sake of consistency with the level of theory used for the GB−CM3 calculations, to which the PB results are compared. Extensive testing[52] demonstrated that it yields accurate results compared to that of higher correlated methods. All ESP charges in the QM region were calculated in the gas phase. This approach is consistent with the evaluation of electrostatic parameters for empirical force fields, most of which are based on ab initio calculations in the gas phase.[53−57] The charge distribution is placed in a cavity with $\epsilon_{QM} = 1$, which is immersed in a continuum dielectric of $\epsilon = 78.4$ representing bulk water. The solvation free energy is then determined by solving the PB equation by using a finite difference method. The atomic radii used to construct the solvent accessible surface (SAS) for H, C, N, and O atoms correspond to the van der Waals (vdW) radii from Bondi.[58] The vdW radius
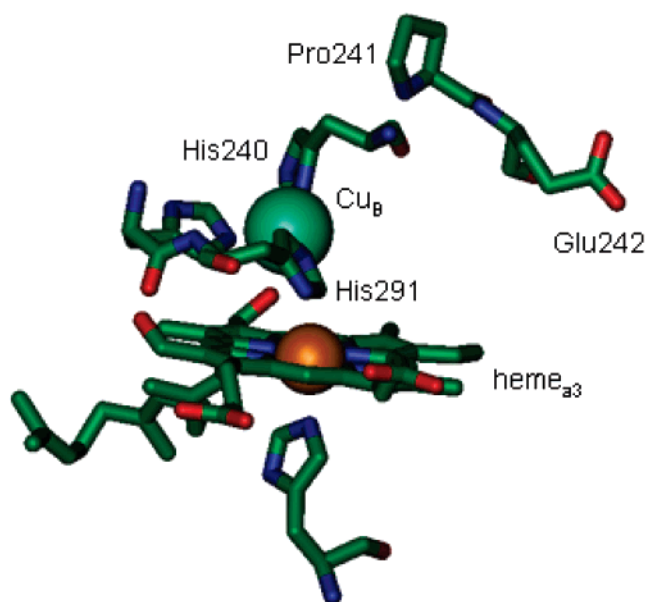
**Figure 7.** Binuclear center of cytochrome *c* oxidase (CcO) from PDB structure 1M56. $Cu_B$ is shown in teal, while Fe of heme$_{a3}$ is shown in orange. Hydrogen atoms were not included in the crystal structure.

for Fe was chosen as 1.456 Å.[59] Because both metals are buried inside the complexes, their vdW spheres do not contribute to the formation of the SAS, so that the precise choice of their vdW radii is not crucial to the accuracy of the solvation free energy. The solvation free energy of the Cu−Fe models in bulk water was determined only with the PB method due to SCF convergence difficulties in the GB-CM3 calculations.

The deprotonation of the $Cu_B$-bound histidine (at pH = 7) within CcO was studied by using continuum electrostatic calculations. The atomic charges for the binuclear center, successively with His291 protonated and deprotonated, correspond to the Singh−Kollman charges calculated for all the large Cu−Fe complexes. These ESP charges are given as Supporting Information. The p$K_a$s were determined successively including only segment A and within all four segments (A, B, C, D) of the bacterial CcO. The protonation state of titratable sites close to His291 could influence the acidity of imidazole. Therefore, we calculated the p$K_a$ values successively with a deprotonated and protonated Glu242. Located at the top of the D-channel, Glu242 has been shown to be a key element in proton translocation. This carboxylic group is thought to function as a relay group shuttling protons from the D-channel to the pocket of the binuclear center.[6,60−66] In the crystal structure of a bacterial CcO (i.e., PDB code 1M56, ref 6), the distance between Glu242 carboxylic oxygen and His291 $N_{\epsilon 2}$ is 11 Å (see Figure 7). The protonation state of Glu242 throughout the catalytic cycle has been the focus of many experimental studies (see refs 67 and 68 and references therein). It has been shown that this carboxylic group has an unusually high p$K_a$ of approximately 9. However, it is not clear if it remains protonated in all the significant catalytic steps.

The protonation state of the other titratable sites in the protein corresponds to their standard state at pH = 7. Subunits A and D are neutral at pH = 7. The few excess charges in subunits B and C (and A when Glu242 is protonated) were neutralized by protonation of solvent-exposed charged residues (e.g., Glu, Asp, and Lys). These residues are located on the cytoplasmic side of the membrane, and they are most likely neutralized by counterions in vivo.

The atomic charges of the residues surrounding the binuclear center correspond to the standard charges in the CHARMM22

**TABLE 1: Solvation Free Energies in Bulk Water ($\epsilon =$ 78.4) for Reference Equilibria (All Energies Are Expressed in kcal·mol$^{-1}$)**

| acid/base | $\Delta G_{sol}^{GB(a)}$ | $\Delta G_{sol}^{PB(b)}$ | $\Delta G_{sol}^{exp(c)}$ | p$K_a^{exp(c)}$ |
|---|---|---|---|---|
| $CH_3CONH_2$/$CH_3CONH^{-1}$ | −60.541 | −69.098 | −70.39 | 15.1 |
| $MeNH_3^{+1}$/$MeNH_2$ | 72.536 | 71.497 | 71.93 | 10.66 |
| PhOH/PhO$^{1-}$ | −58.333 | −59.842 | −64.68 | 9.99 |
| pyridineH$^{+1}$/pyridine | 54.750 | 54.933 | 56.41 | 5.23 |
| $CH_3COOH$/$CH_3COO^{1-}$ | −67.240 | −70.002 | −70.60 | 4.76 |
| $PhNH_3^{+1}$/ $PhNH_2$ | 62.528 | 59.437 | 67.31 | 4.87 |
| $CH_3CONH_3^{+1}$/$CH_3CONH_2$ | 65.840 | 65.051 | 64.09 | −0.66 |

| | mean abs. deviation | | maximum deviation | |
|---|---|---|---|---|
| | $\Delta G_{sol}^{GB}$ | $\Delta G_{sol}^{PB}$ | $G_{sol}^{GB}$ | $G_{sol}^{PB}$ |
| cations | 2.809 | 2.048 | 6.452$^{(d)}$ | 6.007$^{(d)}$ |
| anions | 8.025 | 2.048 | 11.193$^{(e)}$ | 4.335$^{(g)}$ |
| neutral | 1.551 | 0.740 | 2.500$^{(f)}$ | 1.866$^{(h)}$ |

$^a$ Solvation free energy calculated with an SCF generalized Born (GB) approach. $^b$ Solvation free energy calculated with a post-SCF Poisson−Boltzmann (PB) approach. $^c$ Experimental values from ref 76. $^d$ $PhNH_3^{+1}$. $^e$ $CH_3CONH^{-1}$. $^f$ $MeNH_2$. $^g$ PhO$^{1-}$. $^h$ $PhNH_2$.

parameter set.[57] The Cu−Fe models used to derive the ESP-fitted charges describe only a small part of the binuclear center. Hence, all charges used in the continuum electrostatic calculations were rescaled to obtain the appropriate integer value of the total charge. The dielectric constant inside the pocket containing the ab initio-derived charges of the binuclear center is set to $\epsilon_{QM} = 1$. The protein reaction field was represented by a dielectric constant $\epsilon_p$ of 4, which is the value generally used for protein calculations, and repeated with $\epsilon_p = 10$. Recent studies show that, because of water penetration, the polarizability in the protein interior is described more accurately by a uniform continuum dielectric with $\epsilon_p$ between 8 and 12.[69,70−72] Outside of CcO, we set $\epsilon = 80$ with an ionic strength of 150 mM.[73]

All geometry optimizations, energy, vibrational analysis, and ESP charges calculations were performed with GAMESS-US.[74] GB-CM3 calculations were performed with version 4.1 of GAMESSPLUS.[75] The MEAD package[50] was used for the post-SCF PB continuum electrostatic calculations.

## 3. Results

**3.1. Choice of a Reference Acid−Base Couple.** Continuum solvation models commonly used to derive $\Delta G_{solv}$ are able to define very accurately the solvation energy of neutral species. However, the electrostatic field of ionic species strongly perturbs the solvent organization, particularly for solvent molecules in the first solvation shell. These show very different properties compared to the molecules in the bulk, hence can hardly be described by a continuum solvation model. The discrepancy between experiment and continuum electrostatic calculations of ion solvation energies is expected to be in the range of 5 kcal·mol$^{-1}$.[30,43] To select an appropriate reference BH for the calculation of the p$K_a$s within the relative scheme (Figure 5), we tested the accuracy of the GB and PB solvation models in the calculation of the solvation free energy for a few common acid−base couples. The results are shown in Table 1. The largest errors are associated with the solvation free energy of anions. GB shows the largest deviation for the acetamide conjugate base. The equilibrium $MeNH_3^+ \rightarrow MeNH_2$ shows the smallest deviation for the total hydration free energy calculated with both GB ($|\Delta G_{sol}^{GB} - \Delta G_{sol}^{exp}| = 0.606$ kcal·mol$^{-1}$) and PB ($|\Delta G_{sol}^{PB} - \Delta G_{sol}^{exp}| = 0.433$ kcal·mol$^{-1}$) solvation models. For this reason, the couple $MeNH_3^+$/$MeNH_2$ was chosen as reference. The experimental p$K_a$ in bulk water for the deprotonation of $MeNH_3^+$ is 10.66 (ref 40).

**TABLE 2: Calculated p$K_a$s in Bulk Water ($\epsilon = 78.4$) of Isolated 5-Me-imidazole, Imidazolium, and of Cu-bound Imidazole Ring in Various Minimal Cu Models (All Energies Are Expressed in kcal·mol$^{-1}$)**

| acid | $\Delta H_{ele}$ | $\Delta G_{Th}$ | $\Delta G_{sol}^{GB(a)}$ | $\Delta G_{sol}^{PB(b)}$ | p$K_a^{GB}$ | p$K_a^{PB}$ |
|---|---|---|---|---|---|---|
| imidazole | 359.175 | −7.724 | −58.039 | −64.977 | **14.4** | **10.1**[c] |
| imidazolium | 234.416 | −7.846 | 55.404 | 55.730 | **6.1** | **7.1**[d] |
| Cu$^I$[(ImH)$_3$ H$_2$O]$^{+1}$ | 281.271 | −7.733 | 20.217 | 18.799 | **14.7** | **14.4** |
| Cu$^{II}$[(ImH)$_3$ OH]$^{+1}$ | 276.688 | −6.568 | 23.006 | 22.231 | **14.3** | **14.4** |
| Cu$^{II}$[(ImH)$_3$ H$_2$O]$^{+2}$ | 201.285 | −7.179 | 95.225 | 96.972 | **11.5** | **13.5** |
| Reference | | | | | | |
| MeNH$_3^{+1}$ | 224.082 | −8.340 | 72.536 | 71.497 | | *10.66*[e] |

[a] Solvation free energy calculated with an SCF generalized Born (GB) approach. [b] Solvation free energy calculated with a post-SCF Poisson−Boltzmann (PB) approach. [c] The corresponding experimental p$K_a$ value is 14.0.[20−22] [d] The corresponding experimental p$K_a$ value is 7.0.[33] [e] Experimental p$K_a$ from ref 76.

**TABLE 3: Calculated p$K_a$ Values ($\epsilon = 78.4$) of ImH in Various Cu−Fe models in Bulk Water (All Energies Are Expressed in kcal·mol$^{-1}$)**

| | Charge | S$_{tot}$ | $\Delta H_{ele}$ | $\Delta G_{Th}$ | $\Delta G_{sol}^{PB(a)}$ | p$K_a$ |
|---|---|---|---|---|---|---|
| Cu$^{II}$-OH···H$_2$O-Fe$^{III}$ [b] | +2 | 2 | 233.148 | -6.568 | 66.535 | **15.0** |
| Cu$^{II}$-H$_2$O···O=Fe$^{IV}$ | +2 | $\frac{3}{2}$ | 233.405 | -7.179 | 67.932 | **15.8** |
| Cu$^{II}$-OH···Fe$^{II}$ | +1 | $\frac{3}{2}$ | 287.858 | -6.568 | 12.355 | **15.4** |
| Cu$^{II}$-OH···Fe$^{III}$ | +2 | 2 | 236.063 | -6.568 | 65.835 | **16.6** |
| Cu$^{II}$-OH···Fe$^{III}$ | +2 | 3 | 229.432 | -6.568 | 69.655 | **14.8** |

[a] Solvation free energy calculated with a post-SCF Poisson−Boltzmann (PB) approach. [b] The boxes around "Cu" and "Fe" stand to indicate the presence of the three imidazoles and of NH$_3$ and porphyrin, respectively.

### 3.2. p$K_a$ Values in Bulk Water.

The relative scheme shown in Figure 5 was tested successively on the deprotonation of imidazole, which has an anionic conjugate base (i.e., C$_3$N$_2$H$_4$ + H$_2$O → C$_3$N$_2$H$_3^-$ + H$_3$O$^+$), and on the deprotonation of imidazolium, which has a neutral conjugate base (i.e., C$_3$N$_2$H$_5^+$ + H$_2$O → C$_3$N$_2$H$_4$ + H$_3$O$^+$). The experimental p$K_a$s reported in the literature are 14 (refs 20−22) and 7.0 (ref 33) for imidazole and imidazolium, respectively. The results are shown in Table 2. For the deprotonation of imidazole, we obtain very accurate results with GB (p$K_a$ = 14.4), while the PB model significantly overestimates the imidazole acidity, assigning a p$K_a$ of 10.1. The opposite trend is shown in the deprotonation of imidazolium, where GB slightly underestimates the p$K_a$, whereas PB shows very good accuracy.

The results obtained for imidazole as a ligand in different Cu models are also shown in Table 2. For the deprotonation of ImH in a Cu model with copper in its reduced state (i.e., Cu$^I$), we obtain a p$K_a$ of 14.7 with the GB model, and 14.4 with the PB model. The agreement between the two solvation methods is most likely due to their similar level of accuracy in describing the solvation of neutral species and cations (see Table 1). If we compare these results with the ones obtained for the isolated imidazole (p$K_a^{exp} \approx 14$), it is clear that the presence of the metal does not have any significant effect on the acidity.

Two Cu models with copper in its oxidized state (Cu$^{II}$) were studied. In the first complex, Cu$^{II}$ is bound to three imidazoles rings and one hydroxyl, making the total charge of the acid form equal to +1. In the other complex, the metal is ligated to a water molecule as fourth ligand, so that the total charge of the acid form is +2. The p$K_a$ of the imidazole ring in the [ImH]$_3$Cu$^{II}$−OH complex is very close to the one calculated for the [ImH]$_3$Cu$^I$−H$_2$O despite the different oxidation state of the metal. An increase in acidity is calculated for the [ImH]$_3$Cu$^{II}$−H$_2$O complex. The results obtained with the GB model show a decrease of 2.8 p$K_a$ units compared to the [ImH]$_3$Cu$^{II}$−OH complex. A less significant decrease of 0.9 p$K_a$ units is obtained

when using the PB solvation model. This change in acidity could be due to the fact that the [ImH]$_3$Cu$^{II}$−H$_2$O complex is charged in both protonated (+2) and deprotonated (+1) forms, whereas both of the other two complexes have neutral conjugate bases.

The effect of the high-spin Fe$_{a3}$ group on the acidity of ImH was investigated through the study of different Cu−Fe complexes (see Figure 3). Each of the Cu−Fe models is designed to reproduce a stage in the CcO catalytic cycle to assess the possibility of a deprotonation of ImH linked to a proton pumping event. Because complexes of Cu$^I$ do not participate in pumping events, in all of the Cu−Fe complexes studied, Cu is in its oxidized state (i.e., Cu$^{II}$). The calculated p$K_a$ values are shown in Table 3. The inclusion of the Fe−porphyrin results in an increase of the imidazole p$K_a$ values, independently of the nature of the intermetal ligands or the Fe redox state. The calculated p$K_a$s are in the range of 14.8−16.6. The lowest p$K_a$ value corresponds to the hypothetical ferromagnetic (S = 3) model of the O-state,

$$\boxed{Cu^{II}}\text{-OH}\cdots\text{H}_2\text{O-}\boxed{Fe^{III}}$$
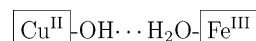
(the boxes around "Cu" and "Fe" indicate the presence of the three imidazoles, and of NH$_3$ and porphyrin, respectively), which we are considering in our calculations in order to determine the effect of magnetic coupling on the acidity of Cu-bound imidazoles. The highest p$K_a$ value corresponds to the antiferromagnetic state (S = 2).

$$\boxed{Cu^{II}}\text{-OH}\cdots\text{H}_2\text{O-}\boxed{Fe^{III}}$$
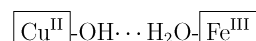
The p$K_a$ values determined for the Cu− and Cu−Fe complexes in bulk water can be used in eq 2 to obtain the proton solvation free energy ($\Delta G_{sol}^{H^+}$). The results are shown in Table 4. All $\Delta G_{sol}$ data listed refer to the PB calculations for consistency. The average of the $\Delta G_{sol}^{H^+}$ values derived from

**22636**  *J. Phys. Chem. B, Vol. 109, No. 47, 2005*

Fadda et al.

**TABLE 4: Proton Solvation Free Energy ($\Delta G_{Sol}^{H^+}$) Derived from Calculated $pK_a$ Values in Bulk Water (All Energies Are Expressed in kcal·mol$^{-1}$)**

| $pK_a^{(a)}$ | $\Delta H_{gas}^{(b)}$ | $\Delta G_{sol}^{(c)}$ | $\Delta G_{sol}^{H^+}$ |
|---|---|---|---|
| 7.1 | 220.250 | 55.730 | −266.296 |
| 10.1 | 345.131 | −64.977 | −266.378 |
| 14.4 | 267.218 | 18.799 | −266.375 |
| 14.4 | 263.800 | 22.231 | −266.389 |
| 13.5 | 187.786 | 96.972 | −266.344 |
| 15.0 | 220.260 | 66.535 | −266.335 |
| 15.4 | 274.970 | 12.355 | −266.320 |
| 14.8 | 216.544 | 69.955 | −266.311 |
| 16.6 | 223.175 | 65.835 | −266.367 |
| 15.8 | 219.906 | 67.932 | −266.287 |
| average | | | **−266.340** |
| standard deviation | | | **0.036** |

$^a$ $pK_a$ values (from $\Delta G_{sol}^{PB}$) correspond to acid−base couples shown in Tables 2 and 3. $^b$ $\Delta H_{gas} = \Delta H_{ele} + \Delta G_{Th} + H_{trans}^{H^+} + \Delta(pV) - T[S^{H^+}]$. $^c$ $\Delta G_{sol} = \Delta G_{sol}^{A^-} - \Delta G_{sol}^{AH}$.

**TABLE 5: Calculated $pK_a$s of the Cu$_B$-bound Imidazole Ring of His291$^a$**

| | $\Delta G_{sol}^{sub.A(b)}$ | $\Delta G_{sol}^{full(c)}$ | $pK_a^{sub.A}$ | $pK_a^{full}$ |
|---|---|---|---|---|
| | *Deprotonated Glu242* | | | |
| Cu$^{II}$-OH···H$_2$O-Fe$^{III}$ | −197.355 | −197.336 | **16.8** | **16.8** |
| Cu$^{II}$-H$_2$O···O=Fe$^{IV}$ | −194.932 | −195.189 | **18.3** | **18.1** |
| Cu$^{II}$-OH···Fe$^{II}$ | −239.175 | −238.249 | **26.2** | **26.9** |
| Cu$^{II}$-OH···Fe$^{III}$ | −198.069 | −198.233 | **18.4** | **18.3** |
| | $\Delta G_{sol}^{sub.A}$ | $\Delta G_{sol}^{full}$ | $pK_a^{sub.A}$ | $pK_a^{full}$ |
| | *Protonated Glu242* | | | |
| Cu$^{II}$-OH···H$_2$O-Fe$^{III}$ | −198.157 | −199.989 | **16.2** | **14.9** |
| Cu$^{II}$-H$_2$O···O=Fe$^{IV}$ | −195.802 | −198.021 | **17.7** | **16.0** |
| Cu$^{II}$-OH···Fe$^{II}$ | −240.259 | −241.047 | **25.5** | **24.9** |
| Cu$^{II}$-OH···Fe$^{III}$ | −198.921 | −201.020 | **17.8** | **16.2** |

$^a$ Results are shown for deprotonated and protonated Glu242 successively with only subunit A and with all four subunits (full protein), with a protein dielectric constant $\epsilon = 4$. All energies are expressed in kcal·mol$^{-1}$. $^b$ Binuclear center in CcO subunit A only, which is in turn immersed in a continuum of $\epsilon = 80$ with ionic strength 150 mM. $^c$ Binuclear center surrounded by all four subunits (A, B, C, D) of CcO. The protein is immersed in a continuum of $\epsilon = 80$ with ionic strength 150 mM.

each equilibrium is −266.340 kcal·mol$^{-1}$. The corresponding standard deviation is 0.036 kcal·mol$^{-1}$.

**3.3. $pK_a$ Values in Cytochrome $c$ Oxidase.** As shown in Figure 1, the Cu$_B$−heme$_{a3}$ binuclear center is located in a pocket deep inside subunit A of CcO. The effect of the proteic environment on the acidity of the Cu$_B$-bound histidine is studied by combining DFT with PB continuum electrostatics. Tables 5 and 6 list the results obtained via the thermodynamic cycle in Figure 4, in combination with the $\Delta G_{sol}^{H^+} = -266.340$ kcal·mol$^{-1}$ derived from the $pK_a$s in bulk water (see above). The $pK_a$ values listed in Table 5 were obtained successively from calculations including only subunit A and the full protein (i.e., subunits A, B, C, and D in bacterial CcO), and with deprotonated and protonated Glu242. Table 5 shows the results obtained with $\epsilon_p = 4$ to describe the protein reaction field, while Table 6 shows the results obtained with $\epsilon_p = 10$, a value which takes into account the effect of water penetration in the protein interior.[69−71] Compared to the results in bulk water, the consistent effect of the low dielectric proteic environment is to shift the equilibrium toward higher $pK_a$ values. For antiferro-

**TABLE 6: Calculated $pK_a$s of the Cu$_B$-bound Imidazole Ring of His291 with All Four Subunits (Full Protein), with a Protein Dielectric Constant $\epsilon_p = 10^a$**

| | Protonated Glu242 | |
|---|---|---|
| | $\Delta G_{sol}^{full(b)}$ | $pK_a^{full}$ |
| Cu$^{II}$-OH···H$_2$O-Fe$^{III}$ | -198.029 | **16.3** |
| Cu$^{II}$-H$_2$O···O=Fe$^{IV}$ | -196.291 | **17.3** |
| Cu$^{II}$-OH···Fe$^{II}$ | -243.307 | **23.2** |
| Cu$^{II}$-OH···Fe$^{III}$ | -199.402 | **17.4** |

$^a$ All energies are expressed in kcal·mol$^{-1}$. $^b$ Binuclear center surrounded by all four subunits (A, B, C, D) of CcO. The protein is immersed in a continuum of $\epsilon = 80$ with ionic strength 150 mM.

magnetic coupled metals in the binuclear center, the $pK_a$ in CcO ranges from 16.8 to 26.9 with $\epsilon_p = 4$ and deprotonated Glu242. Protonation of Glu242 results in a downshift of $pK_a$ values by an average of 0.5 units when only subunit A is considered, and by 2 units when the whole protein is included in the model system (see Table 5). However, when the protein dielectric constant is increased to $\epsilon_p = 10$, the $pK_a$ values increase again by 1.3 units (on average) for all complexes other than

$$Cu^{II}\text{-OH}\cdots Fe^{II}$$

whose $pK_a$ decreases by 1.7 units. This effect can be understood in terms of the total charge of this complex, which, contrary to the other states studied, has a neutral conjugate basis. Finally, we note that $pK_a$ values of the same order of magnitude as the ones calculated in the protein interior were obtained for the small Cu models by continuum electrostatics in dimethyl sulfoxide (DMSO, $\epsilon = 46.8$). These data are included as Supporting Information. This result is consistent with the previously reported finding that a dielectric constant higher than 2−4 is needed in continuum dielectric calculations in order to obtain $pK_a$ values closer to the ones measured in proteins.[77−79]

## 4. Discussion

Within the framework of a recently proposed pumping mechanism,[14,15,19] the deprotonation of the Cu$_B$-bound H291 is presumed to be triggered by the entry of a chemical proton in the binuclear center, which converts a hydroxyl ligand into a water molecule.[14,15] According to this mechanism, H291 deprotonation takes place without dissociation of the N$_{\epsilon2}$−Cu bond, which results in the formation of an imidazolate anion.

In the present work, various Cu− and Cu−Fe complexes were modeled after the CcO binuclear center at different stages of the catalytic cycle. The $pK_a$ values of the Cu-bound imidazole in these complexes were determined successively in bulk water and within CcO. The results obtained for the small Cu models (Table 2) demonstrate that the effect of the oxidation state of the Cu center does not influence the imidazole $pK_a$. Indeed, both [ImH]$_3$Cu$^I$−H$_2$O and [ImH]$_3$Cu$^{II}$−OH, which bear the same charge, but where the metal is in different redox states, have very similar $pK_a$s. The latter are of the same order of magnitude as the experimentally determined $pK_a$ of 14, corresponding to the deprotonation of an isolated imidazole, and are also in agreement with our value of 14.4 calculated with the GB solvation model. The discrepancy of the corresponding $pK_a$ determined with the PB approach is due to the difficulty intrinsic to continuum solvation models in the description of anionic species. Results from test calculations on common acid−base

Acidity of a Cu-Bound Histidine in Cytochrome *c* Oxidase

*J. Phys. Chem. B, Vol. 109, No. 47, 2005*  **22637**

couples, for which the solvation free energy is known experimentally, show that the solvation of neutral species is very well reproduced by both PB and GB methods (see Table 1). In this particular case, the deviation in the solvation free energy calculated for the imidazolate with PB is probably larger than the one obtained for the GB method, and it is not counterbalanced by a similar deviation in the solvation free energy of the acid. These results emphasize that, because $pK_a$ calculations are extremely sensitive to small energy deviations, solvation free energy contributions should be tested with different levels of theory.

An increase in acidity is determined for the deprotonation of $[ImH]_3Cu^{II}-H_2O$. This behavior can be interpreted in terms of stabilization of charged species in bulk water. Here the acid has a higher charge ($+2$) than that of the other complexes studied. Its deprotonation leads to a charged conjugate base, whereas both of the other two complexes have neutral conjugate bases. One might consider $[ImH]_3Cu^{II}-H_2O$ as produced by the addition of a proton to the hydroxyl ligand of $[ImH]_3Cu^{II}-$OH. According to the proposed pumping mechanism, the imidazole acidity should increase. Indeed, the $pK_a$ value in $[ImH]_3Cu^{II}-H_2O$ is 11.5 (according to the GB model), which is significantly lower than that of $[ImH]_3Cu^{II}-OH$ ($pK_a = 14.3$), whereas the corresponding $pK_a$ downshift calculated with the PB solvation model is only of 0.9 units. Thus, despite the relatively higher acidity of $[ImH]_3Cu^{II}-H_2O$, all Cu−imidazoles complexes studied clearly favor the fully protonated form. This is in agreement with the results of a computational study of $Fe^{II}-His$ $pK_a$ values in the Rieske protein active site.[80] Results show that the acidity of the His side chain bound to $Fe^{II}$ is of the same order of magnitude as that of free methyl−imidazole (i.e., $pK_a$ values in the range of 11.3−12.8). Hence the effect of the ligation to $Fe^{II}$ on His acidity can be considered negligible, and the complexes' fully protonated form is favored. Despite the different stability of $Cu^{II}-$ and $Fe^{II}-His$ complexes,[81] we do also find that the $pK_a$ values of different $Cu^{II}-His$ complexes in bulk water are comparable to that of the free imidazole $pK_a$ (i.e., approximately 14 $pK_a$ units).

Cu models are a very simplistic approximation of the CcO binuclear center. We included the effect of the high-spin Fe−heme$_{a3}$ by studying larger Cu−Fe models with Fe in different oxidation states. We can analyze the results within the framework of the CcO catalytic cycle shown in Figure 2. The different Cu−Fe models were designed to represent the various catalytic steps connected to the deprotonation of the Cu-bound His291. The first deprotonation is expected after the entry of a chemical proton in F to form state $F_p$. The $pK_a$ in bulk water calculated for a model of $F_p$, represented by

$$\boxed{Cu^{II}}\text{-}H_2O\cdots O=\boxed{Fe^{IV}}$$
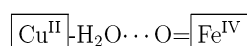
is 15.8, much higher than the $pK_a$ obtained for the corresponding Cu model, $[ImH]_3Cu^{II}-H_2O$.

The next deprotonation is expected in connection with the formation of the O-state, represented by

$$\boxed{Cu^{II}}\text{-}OH\cdots H_2O\text{-}\boxed{Fe^{III}}$$
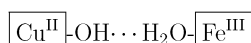
The corresponding $pK_a$ is 15.0. This indicates that the different Fe redox states, consistently with the results obtained for the various Cu redox states, do not cause a significant change on the imidazole $pK_a$. We also tried to study a different model of the O-state, where the water molecule was ligated to Cu, while

the hydroxyl was ligated to Fe. However, the optimization of the intermetal ligands leads inevitably to the complex

$$\boxed{Cu^{II}}\text{-}OH\cdots H_2O\text{-}\boxed{Fe^{III}}$$
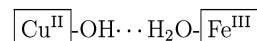
We studied two more states, both with Cu ligated to a hydroxyl as a fourth ligand, and Fe with a free apical coordination site. In the latter configuration, two oxidations states of Fe were considered, Fe $^{III}$ and $Fe^{II}$. Because the hydroxyl can function as a bridging ligand coordinating both Cu and Fe, a ferromagnetic coupling between the two metals can be envisaged, although it should be noted that only antiferromagnetic states ($S = 2$) were identified experimentally.[82] We modeled

$$\boxed{Cu^{II}}\text{-}OH\cdots\boxed{Fe^{III}}$$
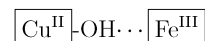
with both ferromagnetic ($S = 3$) and antiferromagnetic ($S = 2$) coupling to gauge the effect of spin coupling on the Cu-bound imidazole $pK_a$. The results in bulk water (Table 3) show that the antiferromagnetic form
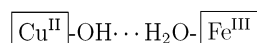
$$\boxed{Cu^{II}}\text{-}OH\cdots\boxed{Fe^{III}}$$
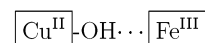
has a $pK_a$ slightly higher than the other complexes, 1.6 units above the value determined for

$$\boxed{Cu^{II}}\text{-}OH\cdots H_2O\text{-}\boxed{Fe^{III}}$$
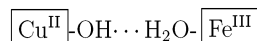
which has the same total charge and oxidation state. The $pK_a$ of the ferromagnetic form

$$\boxed{Cu^{II}}\text{-}OH\cdots\boxed{Fe^{III}}$$
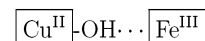
is similar to that of

$$\boxed{Cu^{II}}\text{-}OH\cdots H_2O\text{-}\boxed{Fe^{III}}$$

Given the limits of accuracy of the calculation, the magnetic coupling does not seem to affect the imidazole acidity significantly.

The $pK_a$ values obtained with the PB solvation model for the small Cu models only differ by a few units (up to a maximum deviation of 2.3 $pK_a$ units) from those obtained for the larger Cu−Fe models in bulk water (see Tables 2 and 3). While the Cu models were fully optimized in the protonated and deprotonated form, for Cu−Fe models, only the protonated form was relaxed within the hypothesis that deprotonation was instantaneous. The agreement between the two sets of calculations indicates that structural modifications arising from geometry optimization of the Cu−His complexes have a marginal effect on the acidity of imidazole.

When we consider the Cu−Fe complexes as part of the active site in the protein, the $pK_a$ of the Cu$_B$-bound imidazole ring of H291 shifts to higher values in all relevant catalytic states (see Tables 5 and 6). To gauge the effect of titration of protein side chains on the acidity of H291, in this calculation, we have also taken into account the protonation state of Glu242 (see Table 5). This group is the titratable group closest to His291, and it is thought to play a role in the pumping mechanism.[6,60−66] When we consider only subunit A, the results obtained with a protonated Glu242 are downshifted by only 0.6 $pK_a$ units (on average) relative to the acidities determined when the Glu242 is deprotonated. When we consider all four subunits, this

downshift is on average 2 $pK_a$ units. These $pK_a$ shifts correspond to changes in the total solvation energy of only $0.8-2.8$ kcal·mol$^{-1}$, values which are within the limits of accuracy of continuum solvation models.[30,43] Thus the titration of Glu242 does not have a significant effect on the acidity of His291.

In two recent publications, Quenneville et al.[36] and Popović et al.[37] studied the imidazole acidity in complexes similar to ours. Results were reported for bulk water and in a uniform dielectric of 4,[36] as well as in the proteic environment through continuum electrostatic calculations.[37] Their results in bulk water are similar to ours for [ImH]$_3$Cu$^I$H$_2$O. However, a $pK_a$ of 8.6 was calculated for the oxidized complex [ImH]$_3$Cu$^{II}$H$_2$O, a much lower value than the 11.5 (GB) and 13.3 (PB) we determined. Because the protocol used to calculate the gas-phase energy contribution is essentially the same, the discrepancy in this case is due to relatively small differences (on the order of $2-5$ kcal·mol$^{-1}$) in the solvation energy contribution.

The most significant divergence pertains to the studies in low dielectric and proteic environments. In a uniform continuum dielectric of $\epsilon_p = 4$, the authors report $pK_a$ values of $-9.9$ for a Cu$^{II}$ complex, and 9.8 for a Cu$^I$ complex.[36,37] The protein reaction field was simulated also by including, within the continuum dielectric of $\epsilon = 4$, regions of $\epsilon = 80$ corresponding to protein cavities, which are presumably occupied by internal water.[37] By adding to this heterogeneous reaction field the contribution of protein charges, Popović et al.[37] obtained $pK_a$ values ranging between 2.1 and 4.0 for Cu$^{II}$ complexes, and $17.4-19.7$ for reduced Cu$^I$ complexes. While water penetration is likely to modulate the reaction field of the protein, the basis for modeling internal hydration with dielectric boundaries in continuum electrostatic models is unclear. First, choosing the effective shape and the size of buried cavities is not a trivial matter because the hydration state of cavities is modulated by small changes in the structure and the polarity of the cavity itself.[83] Thus, it is likely that the hydration state of cavities embedded in the interior of redox proteins such as CcO depends on the redox state of the enzyme. In addition, evidence from MD studies suggests that confinement significantly modifies the relaxation dynamics of water molecules in pores and cavities compared to that of bulk water.[84-88] As a result, a dielectric of 80 is inadequate to represent confined water molecules. Finally, the partition of the protein interior into many regions of significantly different dielectric constants can lead to large errors near dielectric boundaries. The reaction field contribution to the free energy of ions in narrow pores was shown to be highly sensitive to the proximity of dielectric boundaries between regions of high and low dielectric.[89] Recent studies suggest that the effect of buried water on the protein reaction field may be incorporated by applying a uniform dielectric constant between 8 and 12 throughout the protein interior.[69-71] In the present study, increasing the dielectric constant of the protein from $\epsilon_p = 4$ to $\epsilon_p = 10$ was found to cause the $pK_a$ values to increase only by 1.4 units on average (see Tables 5 and 6). The only exception is provided by

$$\boxed{Cu^{II}}\text{-OH}\cdots\boxed{Fe^{II}}$$
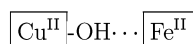
which, contrary to the other complexes, has a neutral conjugate base (see Table 6).

Ultimately, the discrepancy between the results obtained by Popović et al.[37] and by us can be related to three main factors. First, in the previous studies, the $pK_a$ values were calculated relative to the deprotonation of Me−imidazolium in bulk water ($pK_a = 6.6$), even when the reaction takes place in an

environment different from bulk water, such as the uniform dielectric with $\epsilon = 4$, or the CcO protein interior. Yet, on the basis of the thermodynamic cycle depicted in Figure 5, it is clear that, in order to eliminate the dependence from the proton solvation free energy, both equilibria have to take place in the same solvent. Because the expected $pK_a$ value of imidazolium in a low dielectric is presumably higher than 6.6 (e.g., a $pK_a$ value of 10.2 was determined for His63 in thiolsubtilisin Carlsberg[90]), the data reported by Popović et al.[37] are likely to be artificially downshifted. Furthermore, as indicated above, dielectric boundaries separating regions of low dielectric ($\epsilon = 4$ and 1) from regions of high dielectric ($\epsilon = 80$) may cause large fluctuations in the reaction field, which could be critical to the accuracy of acidity calculations if such boundaries are located close to the deprotonation site in the binuclear center. Finally, another significant difference between the present study and that of Popović et al.[37] is that the ESP charges used in their PB calculation for the whole protein were calculated only on the small Cu$_B$ complex, which does not include heme$_{a3}$. As a result, their electrostatic potential may be inappropriate to describe the binuclear center, especially in the intermetal region.

The results that we obtained have important implications for the proposed pumping mechanism. Within the hypothesis of the Cu$_B$-bound H291 imidazole ring as the loading site of the CcO proton pump, we would expect a strong thermodynamic coupling between the redox centers (Cu$_B$ and/or heme$_{a3}$) and the protonation site. This entails a significant dependence of the $pK_a$ of the proton loading site on the redox state of the binuclear center. The calculations performed on Cu models show no significant dependence of $pK_a$ on the Cu oxidation states. When the pumping events take place along the catalytic cycle (see Figure 2), Cu is always present as Cu$^{II}$. The tests conducted in bulk water on larger Cu−Fe complexes, which reproduce more closely the binuclear center, do not support deprotonation of the Cu-bound imidazole. The lower dielectric of the proteic environment has the effect of shifting the already high $pK_a$s to even higher values, indicating a considerable destabilization of the Cu$_B$-bound imidazolate produced by deprotonation within the protein. It is likely that this destabilization would be less dramatic if we had included explicit water molecules in the hydrophobic pocket of the active site. Nevertheless, this refinement of the model would not change our conclusion regarding the absence of thermodynamic coupling between the redox states of the binuclear center and the $pK_a$ of the Cu$_B$-bound imidazole.

It should be noted that a study of $pK_a$, an equilibrium quantity, falls short of the level of detail required to encompass the proton pumping mechanism because pumps work out of equilibrium. The inclusion of transient dynamic events that are likely to play a role in the proton pumping mechanism is beyond the scope of this study. With this caveat in mind, the significance of the $pK_a$ values obtained in the present study resides in the considerable energetic cost associated with deprotonation of the Cu-bound imidazole. For that reason, our findings are inconsistent with a mechanism in which H291 is the key pumping element of the enzyme.

## 5. Conclusions

In this work, we calculated $pK_a$ values for Cu-bound imidazoles in various Cu− and Cu−Fe complexes, with the purpose of assessing the validity of a recently proposed proton pumping mechanism for CcO, based on the deprotonation of a Cu-bound histidine side chain.[14,15] Our approach is based on the study of increasingly more detailed models of CcO binuclear

Acidity of a Cu-Bound Histidine in Cytochrome *c* Oxidase

*J. Phys. Chem. B, Vol. 109, No. 47, 2005* **22639**

center, which allows us to analyze successively the effect of the redox states of Cu, of Cu and Fe, and of the environment surrounding the binuclear center (i.e., bulk water vs enzyme interior). According to the proposed catalytic scheme,[14,15] His291 undergoes deprotonation whenever a chemical proton enters the binuclear center and converts the hydroxyl ligated to one of the metals (Cu or Fe) into water. For this mechanism to work, the imidazole ring p$K_a$ must change considerably depending on the different catalytic steps. Hence, a thermodynamic coupling between the binuclear center redox states and the Cu$_B$-bound imidazole ring acidity is to be expected.

The experimental p$K_a$ value for the deprotonation of imidazole, which produces an anionic imidazolate, is approximately 14.[20-22] Our calculations in bulk water on small Cu complexes do not show any significant change of the p$K_a$ due to the ligation of the imidazole to Cu. Furthermore, the results obtained for Cu$^I$ and Cu$^{II}$ complexes bearing the same total charge do not show any significant dependence on the redox state of the metal.

The study of larger complexes, which include an Fe–porphyrin with Fe in different redox states (i.e., II, III, and IV), representing the heme$_{a3}$ at various stages of the catalysis, reveals a small increase in the p$K_a$ of imidazole. Still, no significant dependence of the imidazole p$K_a$ on the oxidation state of the binuclear center was determined.

Finally, we considered the effect of the protein environment by combining DFT calculations with PB continuum electrostatics. The effect of the proteic environment was to increase further the p$K_a$ values in all complexes, independently of the redox state of the metals. The calculations in protein required the use of an absolute scheme, which takes into account explicitly the contribution proton solvation free energy ($\Delta G_{sol}^{H^+}$). The experimental values attributed to $\Delta G_{sol}^{H^+}$ vary by as much as 12 kcal·mol$^{-1}$. Therefore, for consistency with the calculations in bulk water, we derived our estimate of $\Delta G_{sol}^{H^+}$. We obtained $\Delta G_{sol}^{H^+} = -266.340$ kcal·mol$^{-1}$, in excellent agreement with accurate measurements reported in the literature.[31] This result is significant, especially in view of the difficulties intrinsic in the experimental and computational assessment of $\Delta G_{sol}^{H^+}$ and of the consequent uncertainty on the $\Delta G_{sol}^{H^+}$ value. Our estimate supports the finding that $\Delta G_{sol}^{H^+}$ is much more negative than originally thought.[31]

All the p$K_a$s obtained in bulk water as well as in protein are considerable. The values range between 14.8 and 16.6 in bulk water, and between 14.9 and 26.9 in the protein. Continuum calculations based on static molecular models inherently neglect transient events that are required for kinetic control of the process, giving rise to the directional translocation of protons against an electromotive force. Nevertheless, the present results indicate that the energy needed to deprotonate the Cu-bound histidine is very high, which is inconsistent with its previously proposed role as a key proton loading site for the pump mechanism.

The present study should be seen as a necessary first step in characterizing important aspects of the chemistry and equilibrium properties of the enzyme. Future efforts will focus on examining the interplay between equilibrium properties, such as redox and hydration states, and electron and proton transport events.

### References and Notes

(1) Wikström, M. *Nature* **1977**, *273*, 271.
(2) Gennis, R. B. *Front. Biosci.* **2004**, *1*, 581.
(3) Saraste, M. *Science* **1999**, *283*, 1488.
(4) Ferguson-Miller, S.; Babcock, G. T. *Chem. Rev.* **1996**, *96*, 2889.
(5) Wikström, M. *Curr. Opin. Struct. Biol.* **1998**, *8*, 480.
(6) Svensson-Ek, M.; Abramson, J.; Larsson, G.; Törnroth, S.; Brzezinski, P.; Iwata, S. *J. Mol. Biol.* **2002**, *321*, 329.
(7) Iwata, S.; Ostermeier, C.; Ludwig, B.; Michel, H. *Nature* **1995**, *376*, 660.
(8) Tsukihara, T.; Aoyama, H.; Yamashita, E.; Tomizaki, T.; Yamaguchi, H.; Shinzawa-Itoh, K.; Nakashima, R.; Yaono, R.; Yoshikawa, S. *Science* **1995**, *269*, 1069.
(9) Gennis, R. B. *Biochim. Biophys. Acta* **1998**, *1365*, 241.
(10) Wikström, M.; Jasaitis, A.; Backgren, C.; Puustinen, A.; Verkhovsky, M. I. *Biochim. Biophys. Acta* **2000**, *1459*, 514.
(11) Wikström, M. *Biochim. Biophys. Acta* **2000**, *1458*, 188.
(12) Wikström, M.; Verkhovsky, M. I. *Biochim. Biophys. Acta* **2002**, *1555*, 128.
(13) Wikström, M.; Verkhovsky, M. I.; Hummer, G. *Biochim. Biophys. Acta* **2003**, *1604*, 61.
(14) Popović, D. M.; Stuchebrukhov, A. A. *J. Am. Chem. Soc.* **2004**, *126*, 1858.
(15) Popović, D. M.; Stuchebrukhov, A. A. *FEBS Lett.* **2004**, *566*, 126.
(16) Gennis, R. B. *Proc. Natl. Acad. Sci. U.S.A.* **1998**, *95*, 12747.
(17) Michel, H. *Proc. Natl. Acad. Sci. U.S.A.* **1998**, *95*, 12819.
(18) Olkhova, E.; Hutter, M. C.; Lill, M. A.; Helms, V.; Michel, H. *Biophys. J.* **2004**, *86*, 1873.
(19) Das, T. K.; Gomes, C. M.; Teixeira, M.; Rousseau, D. L. *Proc. Natl. Acad. Sci. U.S.A.* **1999**, *96*, 9591.
(20) Walba, H.; Isensee, R. W. *J. Am. Chem. Soc.* **1955**, *77*, 5488.
(21) Yegil, G. *Tetrahedron* **1967**, *23*, 2855.
(22) Cleland, W. W.; Frey, P. A.; Gerlt, J. A. *J. Biol. Chem.* **1998**, *273*, 25529.
(23) Iwaki, M.; Yakovlev, G.; Hirst, J.; Osyczka, A.; Dutton, P. L.; Marshall, D.; Rich, P. P. *Biochemistry* **2005**, *44*, 4230.
(24) Lodi, P. J.; Knowles, J. R. *Biochemistry* **1991**, *30*, 6948.
(25) Yoshikawa, S.; Shinzawa-Itoh, K.; Nakashima, R.; Yaono, R.; Yamashita, E.; Inoue, N.; Yao, M.; Fei, M. J.; Peters Libeu, C.; Mizushima, T.; Yamaguchi, H.; Tomizaki, T.; Tsukihara, T. *Science* **1998**, *280*, 1723.
(26) Proshlyakov, D. A.; Pressler, M. A.; Babcock, G. T. *Proc. Natl. Acad. Sci. U.S.A.* **1998**, *95*, 8020.
(27) Proshlyakov, D. A.; Pressler, M. A.; DeMaso, C.; Leykam, J. F.; DeWitt, D. L.; Babcock, G. T. *Science* **2000**, *290*, 1588.
(28) Iwaki, M.; Puustinen, A.; Wikström. M.; Rich, P. R. *Biochemistry* **2004**, *43*, 14370.
(29) Koch, W.; Holthausen, M. C. *A Chemist's Guide to Density Functional Theory*, Wiley-VCH: Weinheim, 2000.
(30) Chen, J. L.; Noodleman, L.; Case, D. A.; Bashford, D. *J. Phys. Chem.* **1994**, *98*, 11059.
(31) Liptak, M. D.; Shields, G. C. *J. Am. Chem. Soc.* **2001**, *123*, 7314.
(32) Reiss, H.; Heller, A. *J. Phys. Chem.* **1985**, *89*, 4207.
(33) Lim, C.; Bashford, D.; Karplus, M. *J. Phys. Chem.* **1991**, *95*, 5610.
(34) Marcus, Y. *Ion Solvation*, Wiley: New York, 1985.
(35) Tawa, G. J.; Topol, I. A.; Burt, S. K.; Caldwell, R. A.; Rashin, A. A. *J. Chem. Phys.* **1998**, *109*, 4852.
(36) Quenneville, J.; Popović, D. M.; Stuchebrukhov, A. A. *J. Phys. Chem. B* **2004**, *108*, 18383.
(37) Popović, D. M.; Quenneville, J.; Stuchebrukhov, A. A. *J. Phys. Chem. B* **2005**, *109*, 3616.
(38) Atkins, P. *Physical Chemistry*, 6th ed.; W. H. Freeman & Co.: New York, 1997.
(39) Chipman, D. M. *J. Phys. Chem. A* **2002**, *106*, 7413.
(40) Pliego, J. R., Jr.; Riveros, J. M. *Chem. Phys. Lett.* **2000**, *332*, 597.
(41) Brodskaya, E.; Lyubartsev, A. P.; Laaksonen, A. *J. Phys. Chem. B* **2002**, *106*, 6479.
(42) Toth, A. M.; Liptak, M. D.; Phillips, D. L.; Shields, G. C. *J. Chem. Phys.* **2001**, *114*, 4595.

(43) Hawkins, G. D.; Cramer, C. J.; Truhlar, D. G. *J. Phys. Chem.* **1996**, *100*, 19824.

(44) Stevens, P. J.; Devlin, J. F.; Chabalowski, C. F.; Frisch, M. J. *J. Phys. Chem.* **1994**, *98*, 11623.

(45) Stevens, W. J.; Basch, H.; Krauss, M.; Jasien, P. *Can. J. Chem.* **1992**, *70*, 612.

(46) Cundari, T. R.; Stevens, W. J. *J. Chem. Phys.* **1993**, *98*, 5555.

(47) Hay, P. J.; Wadt, W. R. *J. Chem. Phys.* **1984**, *82*, 299.

(48) Winget, P.; Thompson, J. D.; Xidos, J. D.; Cramer, C. J.; Truhlar, D. G. *J. Phys. Chem. A* **2002**, *106*, 10707.

(49) Thompson, J. D.; Cramer, C. J.; Truhlar, D. G. *J. Comput. Chem.* **2003**, *24*, 1291.

(50) Bashford, D. *Lect. Notes Comput. Sci.* **1997**, *1343*, 233; *Scientific Computing in Object-Oriented Parallel Environments*; Ishikawa, Y., Oldehoeft, R. R., Reynders, J. V. W., Tholburn, M. Eds.; ISCOPE97; Springer: Berlin, 1997.

(51) Singh, U. C.; Kollman, P. A. *J. Comput. Chem.* **1984**, *5*, 129.

(52) Sigfridsson, E.; Ryde, U. *J. Comput. Chem.* **1998**, *19*, 377.

(53) Bayly, C. I.; Cieplack, P.; Cornell, W. D.; Kollman, P. A. *J. Phys. Chem.* **1993**, *97*, 10269.

(54) Breneman, C. M.; Wiberg K. B. *J. Comput. Chem.* **1990**, *11*, 361.

(55) Chirlian, L. E.; Francl, M. M. *J. Comput. Chem.* **1987**, *8*, 894.

(56) Jorgensen, W. L.; Tirado-Rives, J. *J. Am. Chem. Soc.* **1988**, *110*, 165.

(57) MacKerell, J. A. D.; Bashford, D.; Bellot, M.; Dunbrack, J. R. L.; Evanseck, J. D.; Field, M. J.; Fisher, G.; Gao, J.; Guo, H.; Ha, S.; Joseph-McCarthy, D.; Kuchnir, L.; Kuczera, K.; Lau, F. T. K.; Mattos, C.; Michnick, S.; Ngo, T.; Nguyen, D. T.; Prodholm, B.; Reiher, I. W. E.; Roux, B.; Schlenkrich, M.; Smith, J. C.; Stote, R.; Straub, J.; Watanabe, M.; Wiórkiewicz-Kuczera, J.; Yin, D.; Karplus, M. *J. Phys. Chem.* **1998**, *102*, 3586.

(58) Bondi, A. *J. Phys. Chem.* **1964**, *68*, 441.

(59) Baik, M.; Friesner, R. A. *J. Phys. Chem. A* **2002**, *106*, 7407.

(60) Pomès, R.; Hummer, G.; Wikström, M. *Biochim. Biophys. Acta: Bioenerg.* **1998**, *1365*, 255.

(61) Hellwig, P.; Rost, B.; Kaiser, U.; Ostermeier, C.; Michel, H.; Mantele, W. *FEBS Lett.* **1996**, *385*, 53.

(62) Puustinen, A.; Bailey, J. A.; Dyer, R. B.; Mecklenburg, S. L.; Wikström, M.; Woodruff, W. H. *Biochemistry* **1997**, *36*, 13195.

(63) Adelroth, P.; Svensson-Ek, M.; Mitchell, D. M., Gennis, R. B.; Brzezinski, P. *Biochemistry* **1997**, *36*, 13824.

(64) Junemann, S.; Meunier, B.; Fisher, N.; Rich, P. R. *Biochemistry* **1999**, *38*, 5248.

(65) Rich, P. R.; Breton, J.; Junemann, S.; Heathcote, P. *Biochim. Biophys. Acta: Bioenerg.* **2000**, *1459*, 475.

(66) Adelroth, P.; Karpefors, M.; Gilderson, G.; Tomson, F. L.; Gennis, R. B.; Brzezinski, P. *Biochim. Biophys. Acta* **2000**, *1459*, 533.

(67) McMahon, B. J.; Fabian, M.; Tomson F.; Causgrove, T.; Bailey, J. A.; Rein, F. N.; Dyer, R. B.; Palmer, G.; Gennis, R. B.; Woodruff, W. H. *Biochim. Biophys. Acta* **2004**, *1655*, 321.

(68) Gennis, R. B. *FEBS Lett.* **2003**, *555*, 2.

(69) Damjanović, A.; García-Moreno, B.; Lattman, E. E.; García, A. E. *Proteins* **2005**, *60*, 433.

(70) Archontis, G.; Simonson, T. *Biophys. J.* **2005**, *88*, 3888.

(71) Dwyer, J. J.; Gittis, A. G.; Karp, D. A.; Lattman, E. E.; Spencer, D. S.; Stites, W. E.; García-Moreno, B. *Biophys. J.* **2000**, *79*, 1610.

(72) Thompson, J. D.; Cramer, C. J., Truhlar, D. G. *J. Phys. Chem. A* **2004**, *108*, 6532.

(73) Bashford, D.; Karplus, M. *Biochemistry* **1990**, *29*, 10219.

(74) Schmidt, M. W.; Baldridge, K. K.; Boatz, J. A.; Elbert, S. T.; Gordon, M. S.; Jensen, J. H.; Koseki, S.; Matsunaga, N.; Nguyen, K. A.; Su, S. J.; Windus, T. L.; Dupuis, M.; Montgomery, J. A. *J. Comput. Chem.* **1993**, *14*, 1347.

(75) Pu, J.; Thompson, J. D.; Xidos, J. D.; Li. J.; Zhu, T.; Hawkins, G. D.; Chuang, Y.-Y.; Fast, P. L.; Liotard, D. A.; Rinaldi, D.; Gao, J.; Cramer, C. J.; Truhlar D. G. *GAMESSPLUS*, version 4.1; University of Minnesota: Minneapolis, 2003.

(76) Pliego, J. R., Jr.; Riveros, J. M. *Phys. Chem. Chem. Phys.* **2002**, *4*, 1622.

(77) Dwyer, J. J.; Gittis, A. G.; Karp, D. A.; Lattman E. E.; Spencer, D. S.; Stites, W. E.; García-Moreno E. B. *Biophys. J.* **2000**, *79*, 1610.

(78) Antosiewicz, J.; McCammon, J. A.; Gilson, M. K. *J. Mol. Biol.* **1994**, *238*, 415.

(79) Antosiewicz, J.; McCammon, J. A.; Gilson, M. K. *Biochemistry* **1996**, *35*, 7819.

(80) Ullmann, G. M.; Noodleman, L.; Case, D. A. *J. Biol. Inorg. Chem.* **2002**, *7*, 632.

(81) Sjöberg, S. *Pure Appl. Chem.* **1997**, *69*, 1549.

(82) Ghilardi, R. A.; Huang, H. W.; Moënne-Laccoz, P.; Stasser, J.; Balckburn, N. J.; Woods, A. S.; Cotter, R. J.; Incarvito, C. D.; Rheingold, A. L.; Karlin, K. D. *J. Biol. Inorg. Chem.* **2005**, *10*, 63.

(83) Vaitheeswaran, S.; Yin, H.; Rasaiah, J. C.; Hummer, G. *Proc. Natl. Acad. Sci. U.S.A.* **2004**, *101*, 17002.

(84) Allen, T. W.; Kuyucak, S.; Chung, S. H. *J. Chem. Phys.* **1999**, *111*, 7985.

(85) Tieleman, D. P.; Berendsen, H. J. C. *Biophys. J.* **1998**, *74*, 2786.

(86) Green, M. E.; Lu, J. *J. Phys. Chem. B* **1997**, *101*, 6512.

(87) Sansom, M. S. P.; Smith, G. R.; Adcock, C.; Biggin, P. C. *Biophys. J.* **1997**, *73*, 2404.

(88) Pomès, R.; Roux, B. *Biophys. J.* **2002**, *82*, 2304.

(89) Chakrabarti, N.; Roux, B.; Pomès, R. *J. Mol. Biol.* **2004**, *343*, 493.

(90) Kahyaoglu, A.; Jordan, F. *Protein Sci.* **2002**, *11*, 965.